

www.acsmaterialslett.org

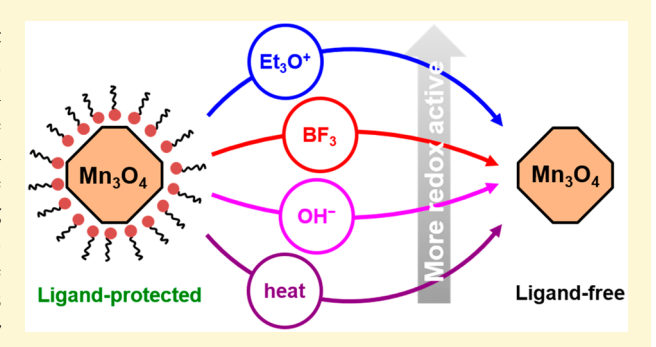
# **Assessment of Soft Ligand Removal** Strategies: Alkylation as a Promising Alternative to High-Temperature Treatments for Colloidal Nanoparticle Surfaces

Andrew Nelson, † Yixu Zong, † Kevin E. Fritz, † Jin Suntivich, \*\*, †, ‡ and Richard D. Robinson\*\*, †

Supporting Information

Downloaded by CORNELL UNIV at 20:28:28:311 on June 30, 2019 from https://pubs.acs.org/doi/10.1021/acsmaterialslett.9b00089.

ABSTRACT: Advances in nanocrystal syntheses over the past decades now enable routine manipulation of particle shape, size, and chemistry with unprecedented precision. Building on decades of knowledge in colloidal chemistry, researchers have created notable high-performance, low-cost energy conversion catalysts. However, in almost all cases, controlling the surface chemistry—in particular, removing the surfactants used during the syntheses—is a challenge. Aggressive physical treatments, such as thermal pyrolysis and plasma etching, have become the methods of choice, but these processes test the material's phase and chemical stability. In this work, we analyze softer methods to postsynthetically remove surfactants using



chemical treatments. We performed various surface treatments to deprotect colloidal nanocrystals of a well-known electrocatalyst, manganese oxide (Mn<sub>3</sub>O<sub>4</sub>), passivated with hydrophobic ligands. We employed a suite of characterization techniques (transmission electron microscopy, infrared spectroscopy, voltammetry, and thermogravimetric analysis) to evaluate their surface chemistry. Although the four studied treatments (bases, alkylating agents, Lewis acids, or heat) could remove nearly all organic ligands, the surface chemistries of the treated nanomaterials differed significantly from treatment to treatment. These chemical differences arise from the reactions between the treatment agent and the surfactant or from side reactions of the agent with atmospheric water or carbon dioxide, leaving behind residues, such as hydrolyzed ligand removal agent, metal hydroxide, and metal carbonate, on the surface. From our study, we find that treatment using alkylating agents is the most promising approach for soft room-temperature stripping of nanocrystal ligands, producing Mn<sub>3</sub>O<sub>4</sub> with the highest electrochemical activity.

¶ he search for high-performance, inexpensive, and scalable catalysts for renewable energy storage and conversion is one of the biggest challenges facing the scientific community in the 21st century. Being a surface phenomenon, heterogeneous (electro)catalysis relies on a solid catalyst, whose surface chemistry still presents a formidable obstacle to optimization. To explain catalyst performance in terms of parameters, such as particle size and surface orientation, well-defined model systems must be prepared: that is, nanoparticles with sharp size distributions and welldefined shape must be isolated. Thus far, the best strategies for preparing size-controlled nanoparticles have come from research on colloidal nanocrystals (NCs), where solution chemistry can tightly control morphology (size, shape, and surface orientation), stoichiometry, and electronic properties.<sup>1,2</sup> In addition to allowing size effects to be assessed, the monodispersity afforded by the NC syntheses can allow the assignment of activities to specific crystal planes.

Current NC syntheses require metal-binding surfactants, that is, ligands, to control particle solubility, growth rates, and relative surface energies.<sup>3</sup> For applications requiring pristine surfaces, the ligands (usually hydrocarbons functionalized with polar head groups) must be removed, as otherwise they could interfere with the catalyst performance. For example, in electronic devices, the ligands are insulating and can prevent electron transfer to/from the particles.4-6 In catalysis, the ligands can block the catalysts from participating in the reaction.<sup>7,8</sup> While numerous protocols for physically or

Received: April 2, 2019 Accepted: June 11, 2019 Published: June 11, 2019



Department of Materials Science and Engineering, Cornell University, Ithaca, New York 14853, United States \*Kavli Institute at Cornell for Nanoscale Science, Cornell University, Ithaca, New York 14853, United States

chemically removing ligands from NCs have been studied, such as thermal annealing, ligand displacement through chemical treatment, 10-12 ligand leaching into excess solvent, 13 plasma cleaning, 14,15 and electrochemical activation, 7,16 their efficacies were often studied in isolation. As a result, it is unclear how effective the removal methods are compared to each other.

In this work, we compare four methods for ligand removal. We focus on postsynthetic chemical treatments with inorganic base, alkylating agent, or Lewis acid and with heat (Figure 1).

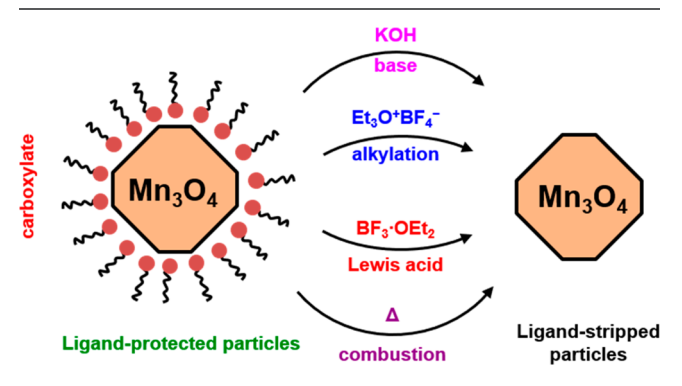


Figure 1. Schematic of surface treatments to remove ligands from metal oxide surfaces for electrocatalysis. Four popular ligand removal strategies were evaluated: bases (potassium hydroxide) displace ligands, for example, with hydroxyl groups; alkylating agents (triethyloxonium tetrafluoroborate) displace carboxylate ligands by esterification; Lewis acids (boron trifluoride as diethyl ether complex) form dative bonds with ligands; and heating in air (300°C) removes ligands by combustion.

We term these procedures the "base", "alkylation", "Lewis acid", and "thermal" methods, respectively. We focus on manganese(II, III) oxide (Mn<sub>3</sub>O<sub>4</sub>), a well-known electrocatalyst for several electrochemical reactions, as our model system. Mn<sub>3</sub>O<sub>4</sub> and other Mn oxides has been investigated by many groups for their oxygen reduction reaction (ORR) and oxygen evolution reaction (OER) activity. 17-22 Both ORR and OER are of critical importance to future renewable electrochemical energy technologies and have been exhaustively researched because of the lack of a suitable high-activity, lowcost replacement for Pt-based catalyst systems. <sup>23-26</sup> Mn<sub>3</sub>O<sub>4</sub> and related Mn oxides have recently stood out among some of the possible candidates for Pt replacement. <sup>17–22</sup> In addition to being inexpensive and nontoxic metal oxides, Mn oxides also have been targeted by nanoparticle synthesis groups, and several colloidal synthesis approaches have been found.<sup>27–31</sup> Mn-oxides are thus a relevant model system for our surface chemistry studies.

We show through transmission electron microscopy (TEM) that the model oxide NC morphology and crystal phase are stable when treated with the four studied strategies. However, their surface chemistries are clearly different, as shown by infrared spectroscopy, cyclic voltammetry, and thermal analyses, implying each treatment is associated with a particular set of side reactions or surface changes. Thermal treatment is effective at cleaning off surface ligands; however, heat-treating the NCs also results in agglomeration of nanoparticles and loss in electrochemically active surface area. Chemical treatments with base and Lewis acid leave residual contaminants and blocking layers that can reduce effective surface area. Alkylation offers a way to avoid both thermal and chemical degradation, making it an effective

treatment protocol for future studies on nanocrystal catalysts. Our systematic examination of post-synthetic chemical strategies for cleaning the NC surface provides a guideline on how to enhance the NC surface reactivity and emphasizes a need for surface characterization methods to understand the nature of the NC surface chemistry beyond bulk parameters.

The base method uses the metathesis reaction between the carboxylate-passivated surface and an inorganic base, such as potassium hydroxide (KOH) in alcohol solution.

$$M(RCOO^{-}) + OH^{-} \rightarrow M(OH^{-}) + RCOO^{-}$$

Here, R is a hydrocarbon group (C<sub>17</sub>H<sub>33</sub> for oleate ligands used here). Reaction with small-molecule bases has been used for phase transfer of nanocrystals from nonpolar to polar solvents, <sup>12,32</sup> removal of ligands from NCs for electronic applications, <sup>4,33</sup> and in our own work for ligand stripping. <sup>34,35</sup>

In the second method, an alkylating agent is used to strip the ligands by esterification of the COO<sup>-</sup> moiety, for example by ethylation with triethyloxonium tetrafluoroborate (Et<sub>3</sub>OBF<sub>4</sub>)<sup>10</sup>

$$M(RCOO^-) + Et_3OBF_4 \rightarrow M(BF_4^-) + Et_2O + RCOOEt$$

This method has been used for removing ligands from a variety of NC surface chemistries and for solubilizing hydrophobic NCs in polar solvents, 10 but its impact on surface electrochemistry is unknown.

The third method, which has been used for the same purposes as the alkylation method, abstracts the ligands by reaction of the Lewis-basic carboxylate group with a Lewis acid, followed by displacement of the complex with solvent molecules. An example is the reaction of oleate-protected surfaces with boron trifluoride (as the etherate)<sup>11</sup>

$$M(RCOO^{-}) + Et_2O \cdot BF_3 \rightarrow M + Et_2O + (RCOO \cdot BF_3)^{-}$$

Finally, ligands may be removed from NCs by combustion in air at high temperatures (>200 °C, thermal method). This method has been frequently used for preparation of oxide electrocatalysts<sup>36–38</sup> and for removing ligands from noble metal surfaces.<sup>7–9</sup> While this method can be said to be a "gold standard," the use of such extreme oxidizing conditions can strongly alter the surface chemistry of the NCs because elevated temperature may induce unintended structural transitions and, in the case of multi-component NCs, alter compositional distributions. High temperatures may also affect particle morphology by sintering, thereby reducing the surface area, <sup>8,9</sup> and decompose a metastable phase, thereby preventing an exploration of novel electrocatalysts that may not necessarily be at the room-temperature ground state.<sup>34</sup>

To assess the impact of these methods on the surface chemistry and morphology of electrocatalytic materials, we synthesized colloidal Mn<sub>3</sub>O<sub>4</sub> NCs by addition of water to manganese acetate in the presence of oleylamine and oleic acid in xylene.<sup>27</sup> For electrochemical testing, Mn<sub>3</sub>O<sub>4</sub> NCs were dispersed on carbon black (Vulcan XC-72) in a 1:1 mass ratio by mechanically mixing the two in hexane,<sup>36</sup> producing a Mn<sub>3</sub>O<sub>4</sub>/C composite.<sup>39</sup> All samples undergo one of the following ligand-removal protocols: for the base procedure, samples were suspended in a 0.1 M KOH isopropanol solution at a concentration of 1-5 mg mL<sup>-1</sup>; for alkylation and Lewis acid treatments, samples were treated with a 1:1 mass ratio of NC or composite to ligand-removal agent in acetonitrile; and for thermal treatment, samples were heat-treated in air at 300 °C for 1 h. Experimental procedures and materials are given in more detail in the Supporting Information.

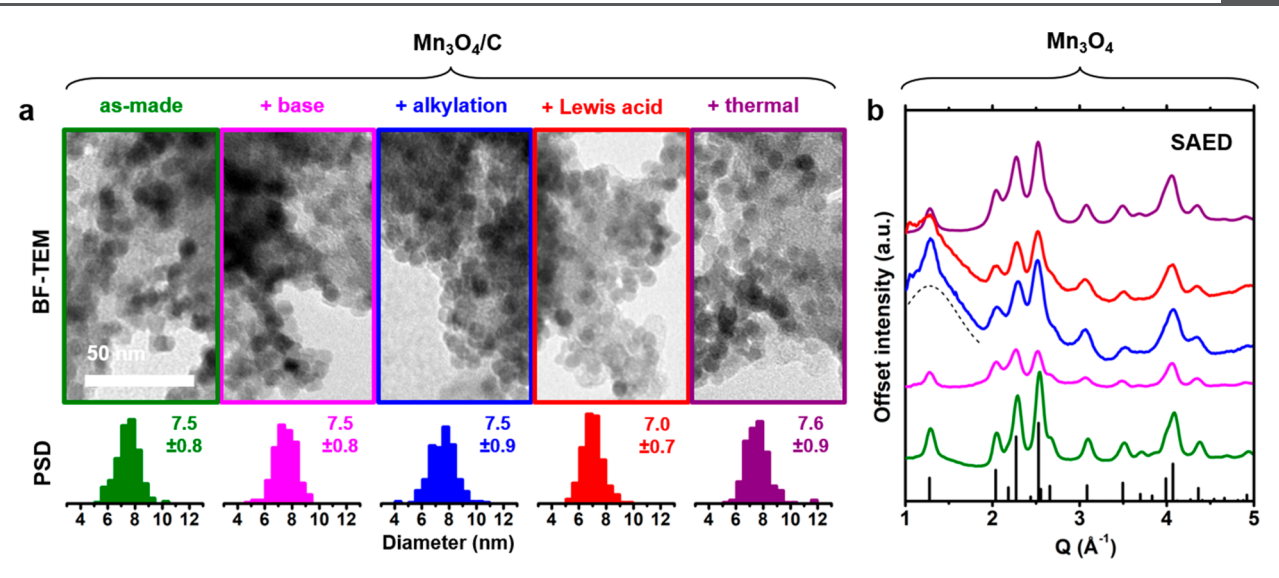


Figure 2. Transmission electron microscopy assessment of morphology and structure of  $Mn_3O_4$  nanocrystals subjected to various treatments. (a) Nanocrystals supported on carbon in bright field TEM (BF-TEM, top), along with particle size distribution (PSD) histograms (N > 300) of measured particle diameters (bottom). Chemical or thermal treatment leaves morphology and size largely unaffected with one exception (Lewis acid). (b) Selected area electron diffraction (SAED) patterns from unsupported nanocrystals. Structure is likewise unchanged following treatment. The stick diagram gives the positions for bulk  $Mn_3O_4$ , hausmannite (JCPDS 01-074-6605), and the dashed line shows a broad peak at  $Q = 1.23 \text{ Å}^{-1}$  (d = 5.11 Å). Curves have been offset for clarity.

TEM was used to determine effects on particle size and shape following treatment of the Mn<sub>3</sub>O<sub>4</sub>/C composites. TEM images of the Mn<sub>3</sub>O<sub>4</sub>/C composites show distinguishable spherical NCs atop the amorphous carbon support. No sign of shape change was observed in the studied treatments (Figure 2a, top). The as-synthesized narrow particle size distributions ( $\sim$ 10% relative standard deviation = the standard deviation divided by the mean, Figure 2a, bottom) were maintained with little change in size. Although a small degree of faceting cannot be ruled out at this resolution, the Mn<sub>3</sub>O<sub>4</sub> NCs appear to be stable after the ligand-removal processes. BF3 treatment is an exception: a small decrease in diameter from 7.5 to 7.0 nm (20% decrease in particle volume) was observed. The mechanism by which metal oxides, such as Mn<sub>3</sub>O<sub>4</sub>, would be dissolved in this way can be explained by considering that the proton may be produced by hydrolysis of BF3 if there was adventitious water in the atmosphere

$$4BF_3 + 3H_2O \rightarrow 3HBF_4 + B(OH)_3$$

Having shown that the NC morphology is stable, we next examine the crystal structure after each chemical treatment.  $MnO_x$  can exist as a number of phases, including  $MnO_s$ ,  $Mn_5O_8$ ,  $Mn_3O_4$ ,  $Mn_2O_3$ , etc.  $^{41-43}$  To determine the crystalline phase, we examined the selected area electron diffraction (SAED) patterns from the NC ensembles following ligand removal. To avoid the contribution from carbon, we prepared films of unsupported Mn<sub>3</sub>O<sub>4</sub> NCs directly on the TEM grids and performed the ligand removal procedures on these films. SAED patterns from the as-prepared NCs are in good agreement with the tetragonal Mn<sub>3</sub>O<sub>4</sub> hausmannite structure (JCPDS 01-074-6605, Figure 2b). As we observed no change in the peak positions, we conclude that the phase of the NCs is stable in the presence of the ligand-removal agents used in this study. Interestingly, for alkylation and Lewis acid treatments, we observed a broad peak at an approximate momentum transfer  $Q = 1.23 \text{ Å}^{-1}$ , corresponding to an interplanar distance of d = 5.11 Å. Because this peak appears only with the

alkylation (containing  $BF_4^-$ ) or Lewis acid (containing  $BF_3$ ) treatments, we suggest that hydrolysis of the boron fluoride species (which is known to occur over time when the storage conditions are imperfect <sup>40,44</sup>) produces an amorphous residue contributing to scattering observed in SAED. However, we are not able to assign an exact structure to this feature at this time.

We observe that alkylating agents or Lewis acids can etch unsupported Mn<sub>3</sub>O<sub>4</sub> NCs. Specifically, the diameter of the Mn<sub>3</sub>O<sub>4</sub> NCs decreased from 6.9 to 4.8 and 5.0 nm following the alkylation and Lewis acid exposure, respectively (Figure S1). The pronounced difference in the degree of etching between treatments of Mn<sub>3</sub>O<sub>4</sub>/C versus unsupported Mn<sub>3</sub>O<sub>4</sub> is likely due to differences in the amount of Mn<sub>3</sub>O<sub>4</sub> present. We confirmed this by examining the aggregates produced from NCs treated in solution (Figure S2). In contrast to the NCs deposited directly on a grid, no change in diameter was seen when ligand removal conditions were more similar to those used for preparing Mn<sub>3</sub>O<sub>4</sub>/C composites. It is apparent that when a very small amount of NCs on a TEM grid are treated by immersion in several milliliters of ligand-stripping solution, the excess of alkylating agent or Lewis acid is much larger than in the case of treatment of Mn<sub>3</sub>O<sub>4</sub>/C, where the composite is dispersed at concentrations of 1-5 mg mL<sup>-1</sup>. The etching by the alkylation agent was unexpected, and we suspect that the etching may occur indirectly via the generation of acid following hydrolysis by adventitious water in the atmosphere 44

$$\text{Et}_3\text{O}^+\text{BF}_4^- + \text{H}_2\text{O} \rightarrow \text{Et}_2\text{O} + \text{Et}\text{OH} + \text{HBF}_4$$

We did not observe any preferential etching along specific facets in  $\mathrm{Mn_3O_4}$  NCs. As shown in the TEM images, the samples retained their original spherical morphology after the treatment. For the purpose of this work, the most important observation from TEM is that the shape and phase of NCs appear to be unchanged after the chemical treatment. On the basis of the assessment of the particle size distributions (PSDs) from Figure 2a, we only observed a statistically significant change in NC size for treatment with Lewis acid (p-value  $\sim$ 

10<sup>-15</sup>), while size differences were not significant for other treatments (see Table S1 for particle size statistics). Nonetheless, to exclude the possibility of etching and size change, scrupulously dry conditions and pure reagents must be used. Otherwise, side reactions of the alkylating agent or Lewis acid with adventitious water will produce acids that can dissolve the oxide NCs.

To verify whether the treatments were able to remove the surfactant molecules tethered to the NCs, we utilize a common <sup>7,10–12,35</sup> assay, Fourier transform infrared (FTIR) spectroscopy, to determine the presence or absence of absorption bands arising from these species. For Mn<sub>3</sub>O<sub>4</sub>/C composites, the strong absorption from the carbon support precluded an observation of the mid-IR region. As a result, the FTIR spectra from Figure 3a are given for unsupported NCs. The major peak assignments are given in Table 1. The 3000–2800 cm<sup>-1</sup> band (feature 1) is important, as it corresponds to the C–H stretching vibrations for alkyl and alkene moieties. <sup>45</sup> The absorbance in this region is an indicator of the overall surfactant content. In as-synthesized (ligand-protected) NCs,

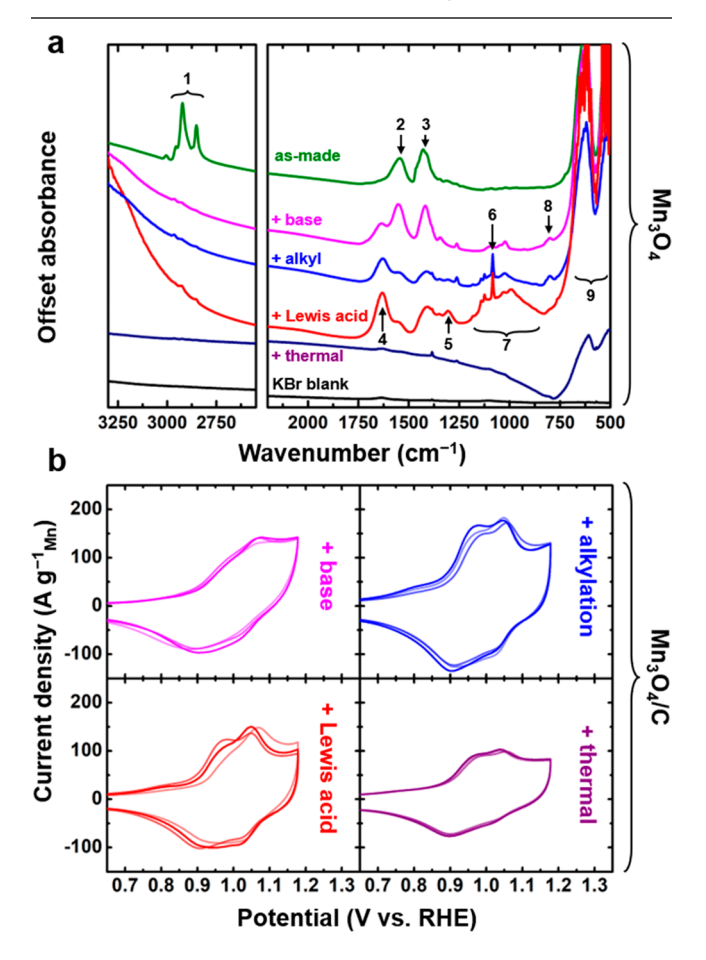


Figure 3. Surface chemistry of  $\rm Mn_3O_4$  nanocrystals subject to various treatments. (a) Fourier transform infrared spectroscopy of unsupported NCs, KBr matrix. Shown are the C–H stretching bands (left) and the lower-frequency skeletal and inorganic bands (right). Curves have been offset for clarity. For peak assignments, see main text. (b) Cyclic voltammetric characterization, with NCs supported on Vulcan XC-72. To show the reproducibility of the measurement, three electrodes are shown for each condition (lighter curves). 0.1 M KOH, Ar-saturated solution; 50 mV s<sup>-1</sup> scan rate.

Table 1. Assignment of Functional Groups from Infrared Bands $^a$ 

feature no.	range (cm <sup>-1</sup> )	width	absent in	strong in	assignment
1	3000- 2800	sharp	T	U	aliphatic C-H stretch
2	1550- 1540	broad	T	UB	asymmetric COO <sup>-</sup> stretch, carbonate
3	1430- 1410	broad	T	UB	symm. COO <sup>-</sup> stretch, carbonate
4	1635- 1625	broad	UT	U	H-O-H bending
5	1310- 1300	broad	UBT	L	B-O stretch
6	1084	very sharp	UBT	AL	BF <sub>4</sub> <sup>-</sup> asymm. B–F stretch
7	1200- 800	very broad	UBT	L	O-H deformation
8	805- 795	sharp	ULT		unknown
9	625- 615	broad		UBALT	Mn-O lattice

 $^{a}$ U = untreated Mn<sub>3</sub>O<sub>4</sub> nanocrystals, B = base-treated, A = alkylation-treated, L = Lewis acid-treated, and T = thermally treated.

peaks from the C–H stretching vibrations were readily visible (Figure 3a, left). As expected from a ligand removal process, all treatments drastically reduce the strength of the C–H peaks, indicating the removal of oleate groups, and the signals completely disappear in the case of thermal treatment. On the basis of this observation, the thermal treatment is likely the most aggressive for removing the organic content from the NCs. However, the generation of inorganic carbon from the pyrolysis cannot be ruled out. <sup>46</sup> Since we did not observe the N–H stretching vibration band, we conclude that the oleylamine used in synthesis is removed during separation of the NCs from the solvent-surfactant mixture used during synthesis.

The FTIR absorption bands at lower wavenumbers (Figure 3a, right) are consistent with residual inorganic species. Features 2 and 3 were observed in all samples with the exception of the thermally treated one. These features most closely correspond to the C–O vibrations from the carboxyl groups. Interestingly, in all chemically treated samples the C–O peaks remain prominent, even though the C–H stretching region indicates that nearly all aliphatic hydrocarbons from the oleate ligands have been removed. Therefore, we hypothesize that such features could arise from carbonate, CO<sub>3</sub><sup>2-</sup>. The particularly strong absorbance of these peaks in the base-treated sample would appear to support this, as KOH is known to take up ambient CO<sub>2</sub>

$$2OH^- + CO_2 \rightarrow HCO_3^- + OH^- \leftrightarrow CO_3^{2-} + H_2O$$

We assign features 4 ( $\sim$ 1630 cm<sup>-1</sup>) and 7 to bending and deformation vibrations from adsorbed water. <sup>45</sup> Both bands are most intense in the Lewis acid-treated sample, indicating the presence of hydroxyl groups either from hydrolyzed BF<sub>3</sub> or adsorbed to the bare oxide surfaces. Additionally, we note that in the base-, alkyl-, and acid-treated samples these two peaks are inversely related to the strength of features 2 and 3. Therefore, we propose that carbonate and water (from the atmosphere or the product of the hydrolysis) competitively adsorb onto the NC surfaces. These "contaminants" form the bulk of the passivation layer on the unsupported NCs.

Features 5 and 6 appear only in the alkyl- and Lewis acid-treated samples. Thus, we assign them to the B–F or B–O vibrations from unreacted and hydrolyzed borate species, respectively. The assignment of feature 5 agrees well with the reported locations for the B–O stretching bands, while the very sharp feature 6 originates from the stable tetrafluor-oborate. A weak peak (feature 8) appears at low energies in both the base- and alkyl-treated samples; because the solution chemistries of these two treatments have no component in common, at present, we are unable to make an assignment to this peak, although it appears to be very minor.

The features (9) at 620 cm<sup>-1</sup> and lower frequencies are observed in all samples. This series of peaks corresponds to the infrared-active vibrational modes of the Mn<sub>3</sub>O<sub>4</sub> lattice, where the precise locations have been reported across a range of values in literature. Our peak positions of 625–610 and 525–505 cm<sup>-1</sup> are in good agreement with the Mn<sub>3</sub>O<sub>4</sub> hausmannite phase, which is consistent with the SAED results. The asymmetric curvature of the baseline in the thermally treated sample is suggestive of a Fano resonance as has been observed in microporous and other nanostructured oxides, but identifying the origin of this phenomenon requires further measurements and is beyond the scope of the present Letter.

In summary, our FTIR measurements show that all treatments examined are effective at removing surface alkyl groups; however, chemical treatments left behind various residues. First, carboxylate groups were apparent, suggesting that Mn<sub>3</sub>O<sub>4</sub> NC surfaces react with CO<sub>2</sub> in the atmosphere or solutions during treatment to form carbonates on the surface. Chemically treated surfaces also react with atmospheric water, as indicated by the observation of adsorbed hydroxyl groups. In the case of alkylation and Lewis-acid-treated NCs, we observe boron-containing residues, which may be detrimental to the electrocatalytic activity.

To analyze the surface chemistry of treated NCs, we examined their surface electrochemical behavior by testing the  $\mathrm{Mn_3O_4}$  redox couples  $^{52,53}$  via cyclic voltammetry (CV) of the composite samples (Figure 3b). We prepared a NC ink for the composites from each treatment  $^{39}$  (see Supporting Information). Three curves are shown for each treatment to show the reproducibility of the measurement. In general, two oxidation/reduction waves were observed at  $\sim 0.95$  and 1.05 V versus the reversible hydrogen electrode (RHE) at pH  $\sim 13$  (0.1 M KOH; see Supporting Information for the determination of this voltage  $^{54}$ ). We compare these redox features to assess the efficacy of the chemical treatment, specifically by integrating the charge underneath the redox waves to approximate the oxide electrochemically active surface area (ECSA).

We normalize the integrated charge (ECSA) by the mass of Mn in the composite as measured by inductively coupled plasma optical emission spectrometry (ICP-OES). This metric controls for a possible catalyst-loading change that may occur during the surface cleaning. We observed that the chemically treated composites had a similar Mn content (approximately 35 wt %). However, the thermally treated Mn<sub>3</sub>O<sub>4</sub>/C was 60 wt % Mn. Because the carbon black used here is, by itself, thermally stable in oxidizing atmospheres well above 300 °C, the observed carbon loss likely arises from catalysis of carbon oxidation by the Mn<sub>3</sub>O<sub>4</sub> NCs. A similar observation has been found with metals, such as Pt, which can greatly lower the temperatures at which carbon supports begin to oxidize. The heat-treated Mn<sub>3</sub>O<sub>4</sub> was found to still be well-dispersed on the support by TEM, and the weight fraction of carbon remained

large; thus, we do not expect that the loss of carbon significantly affects the conductivity and hence the electrochemical accessibility of individual  $\rm Mn_3O_4$  NCs. The specific charge calculations are given in the Supporting Information.

The results of these determinations for all treatments are shown in Table S2. Thermally-treated Mn<sub>3</sub>O<sub>4</sub>, despite producing the least contaminated surfaces by FTIR, showed the smallest specific charge (118  $\pm$  3 C  $g_{Mn}^{-1}$ ) of all treatments. This finding corroborates the common knowledge that while heat treatment can efficiently remove surface ligands, it can have undesirable side effects, such as agglomeration and sintering of nanoparticles. As expected from the clean FTIR, thermally treated Mn<sub>3</sub>O<sub>4</sub> showed well-defined redox waves, indicating that the surface sites are clean. In comparison, the Mn<sub>3</sub>O<sub>4</sub> NCs that underwent alkylation have the largest CV response (specific charge 222  $\pm$  4 C  $g_{Mn}^{-1}$ ) with redox features nearly identical to the CV of the thermally treated Mn<sub>3</sub>O<sub>4</sub>. This finding suggests that ligand detachment by esterification of the ligands produces a surface that is remarkably similar to that following the thermal treatment without causing agglomeration.

Treatment with Lewis acid, BF<sub>3</sub>, produces Mn<sub>3</sub>O<sub>4</sub> with similar CVs to those with alkylation or thermally treated Mn<sub>3</sub>O<sub>4</sub>, but the curves are less reproducible, as indicated by the varying shape of the CVs, and the specific charge (161  $\pm$  4 C  $g_{Mn}^{-1}$ ) is smaller than that for alkylating agent-treated NCs. We conjecture that the Lewis acid treatment based on highly reactive BF<sub>3</sub> produces more degradation products, which are difficult to remove following ligand stripping. The presence of these reactive species could alter the surface redox properties of Mn<sub>3</sub>O<sub>4</sub> NCs. KOH treatment is not as effective for exposing the oxide surfaces as the fluoroborate agents were; the specific charge was the least improved over thermal treatment. KOHtreated Mn<sub>3</sub>O<sub>4</sub>/C also had a less well-defined wave structure, which indicates less-accessible redox sites. In sum, alkylatingagent-treated Mn<sub>3</sub>O<sub>4</sub> had the highest specific charge and produced CV curves that were comparable to those of the thermal-treated Mn<sub>3</sub>O<sub>4</sub>, which indicates that the oxide surfaces were (1) free of contaminating passivants as in the base-treated case and (2) relatively free of reactive or blocking contaminants that were present following treatment with base or Lewis acid. The high ECSA of the Mn<sub>3</sub>O<sub>4</sub> NCs following alkylation is also consistent with the FTIR results that showed that alkylation minimized contamination from carbonates and boron-containing species.

We characterize the presence of the surface ligands (both organic and inorganic) by thermogravimetric analysis (TGA) of Mn<sub>3</sub>O<sub>4</sub> NCs (Fig. 4). NC powders were heated at 5 °C min<sup>-1</sup> under flowing air atmosphere up to 550 °C. The differing surface chemistries of the NCs following various treatments are clearly indicated by the dramatic variation in the TGA curves. Untreated Mn<sub>3</sub>O<sub>4</sub> NCs undergo a single, rapid mass loss at ~180 °C (Figure 4, green curve), which we assign to the decomposition of the organic layer. On the other hand, base, alkylation, and acid treated NCs lose mass more rapidly relative to untreated NCs at temperatures below about 150 °C, probably owing to the slow desorption of the surface water/ solvent molecules that remained as a result of the treatments. We note that we do not expect large amounts of surface water in untreated NCs; as shown by the absence of feature 4 in Figure 3a (green curve), the amount of water in the hydrophobic untreated NCs is small. It has been previously reported that Mn carbonate, MnCO<sub>3</sub>, decomposes around 200

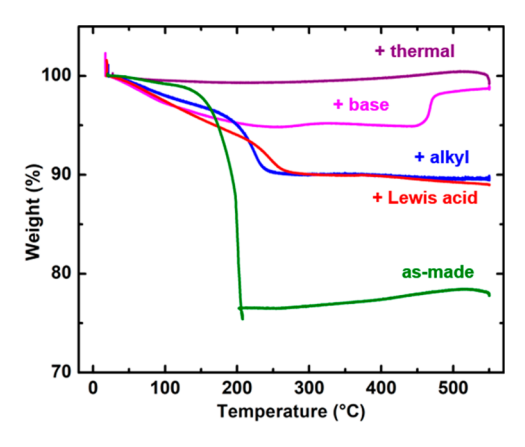


Figure 4. Thermogravimetric analysis in flowing air atmosphere of unsupported  $\rm Mn_3O_4$  nanocrystals subjected to various treatments. Samples were held at room temperature for 15 min, and then the temperature was ramped at 5 °C min <sup>-1</sup> before being held constant at 550 °C for 15 min.

°C, but the reaction is relatively slow. <sup>48,51</sup> Decomposition of MnCO<sub>3</sub> could also contribute to the mass loss, because significant amounts of carbonate remain on the surface of the chemically treated NCs.

The conventional thermal treatment appears to remove all volatile surface molecules, as the TGA measurements indicate that the NCs do not undergo any further mass loss once they are heated to 300 °C, the temperature used for the thermal treatment. Among the treatments studied, the KOH treatment showed the least amount of mass loss in comparison to alkylation and Lewis-acid agent treatments. This observation does not necessarily mean that KOH was the most effective of the chemical treatments at surfactant removal; in fact, the CV and FTIR results indicated the opposite. We explain this observation of low mass loss by pointing out that it is also possible for residual products on the NC surface to react with oxygen and therefore show mass gains in TGA. Mn<sub>3</sub>O<sub>4</sub> NCs treated with alkylation or Lewis-acid agents may have larger mass losses because the residues following treatment decompose to volatile products. Residues in samples treated by KOH may instead be oxidized to form involatile contaminants: KOH-treated Mn<sub>3</sub>O<sub>4</sub> underwent a mass increase at 450-470°C, which can be assigned to an oxygen uptake. 43 The increase in mass at higher temperatures is likely due to the decomposition of a reduced MnO<sub>x</sub>(OH)<sub>y</sub> phase (a hydroxide or oxyhydroxide) to pure Mn oxide at a critical temperature.

α-Mn<sub>2</sub>O<sub>3</sub> (bixbyite) is the stable phase of Mn oxide in air at room temperature up to about 900 °C, whereas MnO or Mn<sub>3</sub>O<sub>4</sub> are only thermodynamically stable under reducing conditions. In the case of our Mn<sub>3</sub>O<sub>4</sub> NCs, it appears this phase transformation is kinetically slow in our TGA experiment, as mass uptake is minimal after 250 °C for all but the base-treated samples. In the case of KOH-treated Mn<sub>3</sub>O<sub>4</sub>, the base treatment likely resulted in a new oxide or oxyhydroxide layer that rapidly decomposed at around 450 °C. Given that the KOH-treated NCs suffer an ECSA loss as measured by CV, this layer may be electrochemically inactive, which could be due to low electronic conductivity. The untreated NCs appear to already exist in their (kinetically) stable oxidation state up to at least 500 °C before ligand stripping. This kinetic stabilization seems to persist in the alkylation, Lewis acid, or

thermal treatments, for which we did not observe any notable redox-state alteration.

In conclusion, we present a systematic evaluation of ligandremoval strategies for colloidal Mn<sub>3</sub>O<sub>4</sub> NCs. We focus on treatments with bases, alkylation agents, Lewis acids, and heat. The effectiveness of each treatment is summarized in Table 2.

Table 2. Effectiveness of Ligand Removal Procedures for Various Surface Chemistry Outcomes<sup>a</sup>

Method	Redox	Carboxyl removal	Bound H <sub>2</sub> O	Volatiles removed
Base				
Alkylation				
Lewis acid				
Thermal				
Most				Least

"Redox = specific charge, carboxyl removal = organic COO" or carbonate CO<sub>3</sub><sup>2-</sup>, and volatiles = total loss after thermogravimetric analysis.

TEM and SAED confirmed that the native oxide NC phases and morphology were stable following all treatments, although for Lewis acid and alkylation treatments a side reaction may occur to create acids that etch the NCs. All treatments were effective in removing the original ligands (oleate) as measured by the C-H stretching vibrations in FTIR. The reactions between the NC surfaces and the chemical reagents, however, leave residual water or metal hydroxides, carbonates, ligandstripping reagent counter ions, and other degradation products. Alkylation agent treatment produced the cleanest NC CVs, comparable to NCs processed by the "gold standard" thermal treatment. However, unlike heat-treated NCs, which had a reduced electrochemical surface area following NC sintering during heat treatment, the NCs undergoing alkylating-agent treatments did not agglomerate. Lewis-acid and KOH treated NCs showed a lower integrated charge density than for the case of alkylation. These two chemical treatments also showed lower reproducibility and poorly defined redox couples during voltammetry. TGA analysis showed that chemical treatments left some volatiles, likely bound water, carbonate, and side reaction products on the NC surface. For KOH treatment, TGA also indicated the likely presence of a partially crystallized oxide or oxyhydroxide layer. Consideration of the factors in Table 2 leads us to conclude that ligand removal by treatment with alkylating agents, such as Et<sub>3</sub>OBF<sub>4</sub>, is the most promising surface-cleaning method, since it produces surfaces as clean as those following heat treatment but does not suffer from possible induced surface area loss or structure alteration. By establishing a new low-temperature cleaning method, our work provides an opportunity to revisit electrochemistry on colloidal redox-active oxide NCs that were previously untested because their ligands could not be removed without resorting to structurally detrimental high-temperature treatments.

### ASSOCIATED CONTENT

## **S** Supporting Information

The Supporting Information is available free of charge on the ACS Publications website at DOI: 10.1021/acsmaterial-slett.9b00089.

Experimental procedures, Figures S1 and S2 (etching or absence thereof in unsupported  $\rm Mn_3O_4$  NCs under different conditions), and Tables S1 and S2 (statistics of nanoparticle size distributions, specific charges) (PDF)

## AUTHOR INFORMATION

# **Corresponding Authors**

\*E-mail: jsuntivich@cornell.edu \*E-mail: rdr82@cornell.edu.

## ORCID ®

Andrew Nelson: 0000-0002-2635-8612 Richard D. Robinson: 0000-0002-0385-2925

#### Notes

The authors declare no competing financial interest.

# ACKNOWLEDGMENTS

This work was supported in part by the National Science Foundation (NSF) under award number CHE-1665305. This work made use of the Cornell Center for Materials Research shared facilities, which are supported through the NSF MRSEC program (DMR-1719875). We also thank D. Zheng (Cornell Materials Science and Engineering) for experimental assistance and S. K. Giri (Cornell Biological and Environmental Engineering) for running ICP-OES tests.

# REFERENCES

- (1) Yin, Y.; Alivisatos, A. P. Colloidal nanocrystal synthesis and the organic—inorganic interface. *Nature* **2005**, *437*, 664–670.
- (2) Jia, C.-J.; Schüth, F. Colloidal Metal Nanoparticles as a Component of Designed Catalyst. *Phys. Chem. Chem. Phys.* **2011**, 13, 2457–2487.
- (3) Boles, M. A.; Ling, D.; Hyeon, T.; Talapin, D. V. The Surface Science of Nanocrystals. *Nat. Mater.* **2016**, *15*, 141–153.
- (4) Rosen, E. L.; Sawvel, A. M.; Milliron, D. J.; Helms, B. A. Influence of Surface Composition on Electronic Transport through Naked Nanocrystal Networks. *Chem. Mater.* **2014**, *26*, 2214–2217.
- (5) Lee, J.-S.; Kovalenko, M. V.; Huang, J.; Chung, D. S.; Talapin, D. V. Band-Like Transport, High Electron Mobility and High Photoconductivity in All-Inorganic Nanocrystal Arrays. *Nat. Nanotechnol.* **2011**, *6*, 348–352.
- (6) Baumgardner, W. J.; Whitham, K.; Hanrath, T. Confined-but-Connected Quantum Solids via Controlled Ligand Displacement. *Nano Lett.* **2013**, *13*, 3225–3231.
- (7) Li, D.; Wang, C.; Tripkovic, D.; Sun, S.; Markovic, N. M.; Stamenkovic, V. R. Surfactant removal for colloidal nanoparticles from solution synthesis: the effect on catalytic performance. *ACS Catal.* **2012**, *2*, 1358–1362.
- (8) Niu, Z.; Li, Y. Removal and utilization of capping agents in nanocatalysis. *Chem. Mater.* **2014**, *26*, 72–83.
- (9) Cargnello, M.; Chen, C.; Diroll, B. T.; Doan-Nguyen, V. V. T.; Gorte, R. J.; Murray, C. B. Efficient removal of organic ligands from supported nanocrystals by fast thermal annealing enables catalytic studies on well-defined active phases. *J. Am. Chem. Soc.* **2015**, *137*, 6906–6911.
- (10) Rosen, E. L.; Buonsanti, R.; Llordes, A.; Sawvel, A. M.; Milliron, D. J.; Helms, B. A. Exceptionally mild reactive stripping of native ligands from nanocrystal surfaces by using Meerwein's salt. *Angew. Chem., Int. Ed.* **2012**, *51*, 684–689.

(11) Doris, S. E.; Lynch, J. J.; Li, C.; Wills, A. W.; Urban, J. J.; Helms, B. A. Mechanistic Insight into the Formation of Cationic Naked Nanocrystals Generated under Equilibrium Control. *J. Am. Chem. Soc.* **2014**, *136*, 15702–15710.

- (12) Nag, A.; Kovalenko, M.; Lee, J.; Liu, W.; Spokoyny, B.; Talapin, D. V. Metal-free inorganic ligands for colloidal nanocrystals: S<sup>2-</sup>, HS<sup>-</sup>, Se<sup>2-</sup>, HSe<sup>-</sup>, Tee<sup>-</sup>, HTe<sup>-</sup>, TeS<sub>3</sub><sup>2-</sup>, OH<sup>-</sup>, and NH<sup>2-</sup> as surface ligands. *J. Am. Chem. Soc.* **2011**, *133*, 10612–10620.
- (13) Lopez-Sanchez, J. A.; Dimitratos, N.; Hammond, C.; Brett, G. L.; Kesavan, L.; White, S.; Miedziak, P.; Tiruvalam, R.; Jenkins, R. L.; Carley, A. F.; Knight, D.; Kiely, C. J.; Hutchings, G. J. Facile Removal of Stabilizer-Ligands from Supported Gold Nanoparticles. *Nat. Chem.* **2011**, *3*, 551–556.
- (14) Shaw, S.; Tian, X.; Silva, T. F.; Bobbitt, J. M.; Naab, F.; Rodrigues, C. L.; Smith, E. A.; Cademartiri, L. Selective Removal of Ligands from Colloidal Nanocrystal Assemblies with Non-Oxidizing He Plasmas. *Chem. Mater.* **2018**, *30*, 5961–5967.
- (15) Aliaga, C.; Park, J. Y.; Yamada, Y.; Lee, H. S.; Tsung, C.-K.; Yang, P.; Somorjai, G. A. Sum Frequency Generation and Catalytic Reaction Studies of the Removal of Organic Capping Agents from Pt Nanoparticles by UV—Ozone Treatment. J. Phys. Chem. C 2009, 113, 6150—6155.
- (16) Solla-Gullón, J.; Montiel, V.; Aldaz, A.; Clavilier, J. Electrochemical Characterisation of Platinum Nanoparticles Prepared by Microemulsion: How to Clean Them without Loss of Crystalline Surface Structure. *Journal of Electroanalytical Chemistry* **2000**, 491, 69–77.
- (17) Gorlin, Y.; Chung, C.-J.; Nordlund, D.; Clemens, B. M.; Jaramillo, T. F.  $Mn_3O_4$  Supported on Glassy Carbon: An Active Non-Precious Metal Catalyst for the Oxygen Reduction Reaction. *ACS Catal.* **2012**, *2*, 2687–2694.
- (18) Huynh, M.; Bediako, D. K.; Nocera, D. G. A Functionally Stable Manganese Oxide Oxygen Evolution Catalyst in Acid. *J. Am. Chem. Soc.* **2014**, *136*, 6002–6010.
- (19) Lima, F. H. B.; Calegaro, M. L.; Ticianelli, E. A. Investigations of the Catalytic Properties of Manganese Oxides for the Oxygen Reduction Reaction in Alkaline Media. *Journal of Electroanalytical Chemistry* **2006**, 590, 152–160.
- (20) Ramírez, A.; Hillebrand, P.; Stellmach, D.; May, M. M.; Bogdanoff, P.; Fiechter, S. Evaluation of  $MnO_{x}$ ,  $Mn_2O_3$ , and  $Mn_3O_4$  Electrodeposited Films for the Oxygen Evolution Reaction of Water. *J. Phys. Chem. C* **2014**, *118*, 14073–14081.
- (21) Gliech, M.; Klingenhof, M.; Görlin, M.; Strasser, P. Supported Metal Oxide Nanoparticle Electrocatalysts: How Immobilization Affects Catalytic Performance. *Appl. Catal., A* **2018**, *568*, 11–15.
- (22) Gorlin, Y.; Jaramillo, T. F. A Bifunctional Nonprecious Metal Catalyst for Oxygen Reduction and Water Oxidation. *J. Am. Chem. Soc.* **2010**, *132*, *13612*–13614.
- (23) Cook, T. R.; Dogutan, D. K.; Reece, S. Y.; Surendranath, Y.; Teets, T. S.; Nocera, D. G. Solar Energy Supply and Storage for the Legacy and Nonlegacy Worlds. *Chem. Rev.* **2010**, *110*, 6474–6502.
- (24) Hong, W. T.; Risch, M.; Stoerzinger, K. A.; Grimaud, A.; Suntivich, J.; Shao-Horn, Y. Toward the Rational Design of Non-Precious Transition Metal Oxides for Oxygen Electrocatalysis. *Energy Environ. Sci.* **2015**, *8*, 1404–1427.
- (25) Yan, D.; Li, Y.; Huo, J.; Chen, R.; Dai, L.; Wang, S. Defect Chemistry of Nonprecious-Metal Electrocatalysts for Oxygen Reactions. *Adv. Mater.* **2017**, *29*, 1606459.
- (26) Man, I. C.; Su, H. Y.; Calle-Vallejo, F.; Hansen, H. A.; Martínez, J. I.; Inoglu, N. G.; Kitchin, J.; Jaramillo, T. F.; Nørskov, J. K.; Rossmeisl, J. Universality in Oxygen Evolution Electrocatalysis on Oxide Surfaces. *ChemCatChem* **2011**, *3*, 1159–1165.
- (27) Yu, T.; Moon, J.; Park, J.; Park, Y. I.; Na, H. B.; Kim, B. H.; Song, I. C.; Moon, W. K.; Hyeon, T. Various-Shaped Uniform Mn<sub>3</sub>O<sub>4</sub> Nanocrystals Synthesized at Low Temperature in Air Atmosphere. *Chem. Mater.* **2009**, *21*, 2272–2279.
- (28) Wang, N.; Guo, L.; He, L.; Cao, X.; Chen, C.; Wang, R.; Yang, S. Facile Synthesis of Monodisperse Mn<sub>3</sub>O<sub>4</sub> Tetragonal Nanoparticles

and Their Large-Scale Assembly into Highly Regular Walls by a Simple Solution Route. *Small* **2007**, *3*, 606–610.

- (29) Sun, X.; Zhang, Y.-W.; Si, R.; Yan, C.-H. Metal (Mn, Co, and Cu) Oxide Nanocrystals from Simple Formate Precursors. *Small* **2005**, *1*, 1081–1086.
- (30) Seo, W. S.; Jo, H. H.; Lee, K.; Kim, B.; Oh, S. J.; Park, J. T. Size-Dependent Magnetic Properties of Colloidal Mn<sub>3</sub>O<sub>4</sub> and MnO Nanoparticles. *Angew. Chem., Int. Ed.* **2004**, *43*, 1115–1117.
- (31) Zhao, N.; Nie, W.; Liu, X.; Tian, S.; Zhang, Y.; Ji, X. Shape- and Size-Controlled Synthesis and Dependent Magnetic Properties of Nearly Monodisperse Mn<sub>3</sub>O<sub>4</sub> Nanocrystals. *Small* **2008**, *4*, 77–81.
- (32) Dong, A.; Ye, X.; Chen, J.; Kang, Y.; Gordon, T.; Kikkawa, J. M.; Murray, C. B. A generalized ligand-exchange strategy enabling sequential surface functionalization of colloidal nanocrystals. *J. Am. Chem. Soc.* **2011**, *133*, 998–1006.
- (33) Otelaja, O. O.; Ha, D.-H.; Ly, T.; Zhang, H.; Robinson, R. D. Highly Conductive Cu<sub>2-x</sub>S Nanoparticle Films through Room-Temperature Processing and an Order of Magnitude Enhancement of Conductivity via Electrophoretic Deposition. *ACS Appl. Mater. Interfaces* **2014**, *6*, 18911–18920.
- (34) Nelson, A.; Fritz, K. E.; Honrao, S.; Hennig, R. G.; Robinson, R. D.; Suntivich, J. Increased Activity in Hydrogen Evolution Electrocatalysis for Partial Anionic Substitution in Cobalt Oxysulfide Nanoparticles. *J. Mater. Chem. A* **2016**, *4*, 2842–2848.
- (35) Zhang, H.; Hu, B.; Sun, L.; Hovden, R.; Wise, F. W.; Muller, D. A.; Robinson, R. D. Surfactant ligand removal and rational fabrication of inorganically connected quantum dots. *Nano Lett.* **2011**, *11*, 5356–5361.
- (36) Guo, S.; Zhang, S.; Wu, L.; Sun, S. Co/CoO nanoparticles assembled on graphene for electrochemical reduction of oxygen. *Angew. Chem.* **2012**, *124*, 11940–11943.
- (37) Wu, L.; Li, Q.; Wu, C. H.; Zhu, H.; Mendoza-Garcia, A.; Shen, B.; Guo, J.; Sun, S. Stable Cobalt Nanoparticles and Their Monolayer Array as an Efficient Electrocatalyst for Oxygen Evolution Reaction. *J. Am. Chem. Soc.* **2015**, *137*, 7071–7074.
- (38) Zhu, H.; Zhang, S.; Huang, Y.-X.; Wu, L.; Sun, S. Monodisperse  $M_xFe_{3-x}O_4$  (M = Fe, Cu, Co, Mn) nanoparticles and their electrocatalysis for oxygen reduction reaction. *Nano Lett.* **2013**, *13*, 2947–2951.
- (39) Suntivich, J.; Gasteiger, H. A.; Yabuuchi, N.; Shao-Horn, Y. Electrocatalytic measurement methodology of oxide catalysts using a thin-film rotating Disk electrode. *J. Electrochem. Soc.* **2010**, *157*, B1263.
- (40) Wamser, C. A. Equilibria in the System Boron Trifluoride—Water at 25°. J. Am. Chem. Soc. 1951, 73, 409-416.
- (41) Grundy, A. N.; Hallstedt, B.; Gauckler, L. J. Assessment of the Mn-O System. *J. Phase Equilib.* **2003**, 24, 21–39.
- (42) Gillot, B.; El Guendouzi, M.; Laarj, M. Particle Size Effects on the Oxidation–Reduction Behavior of Mn<sub>3</sub>O<sub>4</sub> Hausmannite. *Mater. Chem. Phys.* **2001**, *70*, 54–60.
- (43) Al Sagheer, F. A.; Hasan, M. A.; Pasupulety, L.; Zaki, M. I. Low-Temperature Synthesis of Hausmannite Mn<sub>3</sub>O<sub>4</sub>. *J. Mater. Sci. Lett.* **1999**, *18*, 209–211.
- (44) D'Ulivo, A.; Pagliano, E.; Onor, M.; Pitzalis, E.; Zamboni, R. Vapor Generation of Inorganic Anionic Species after Aqueous Phase Alkylation with Trialkyloxonium Tetrafluoroborates. *Anal. Chem.* **2009**, *81*, 6399–6406.
- (45) Socrates, G. Infrared and Raman Characteristic Group Frequencies; John Wiley & Sons: New York, 2001.
- (46) Mohapatra, P.; Shaw, S.; Mendivelso-Perez, D.; Bobbitt, J. M.; Silva, T. F.; Naab, F.; Yuan, B.; Tian, X.; Smith, E. A.; Cademartiri, L. Calcination does not Remove All Carbon from Colloidal Nanocrystal Assemblies. *Nat. Commun.* **2017**, *8*, 2038.
- (47) Ishii, M.; Nakahira, M.; Yamanaka, T. Infrared Absorption Spectra and Cation Distributions in (Mn, Fe)<sub>3</sub>O<sub>4</sub>. *Solid State Commun.* **1972**, *11*, 209–212.
- (48) El-Shobaky, G. A.; Ghozza, A. M.; Hassan, H. A. Thermal Decomposition of Manganese Carbonate Supported on Active Alumina. *J. Therm. Anal. Calorim.* **1998**, *51*, 529–539.

- (49) Shang, G. L.; Fei, G. T.; Zhang, Y.; Yan, P.; Xu, S. H.; Ouyang, H. M.; De Zhang, L. Fano Resonance in Anodic Aluminum Oxide Based Photonic Crystals. *Sci. Rep.* **2015**, *4*, 3601.
- (50) Banerjee, S.; Kim, D.-I.; Robinson, R. D.; Herman, I. P.; Mao, Y.; Wong, S. S. Observation of Fano Asymmetry in Raman Spectra of SrTiO<sub>3</sub> and Ca<sub>x</sub>Sr<sub>1-x</sub>TiO<sub>3</sub> Perovskite Nanocubes. *Appl. Phys. Lett.* **2006**, *89*, 223130.
- (51) Reidies, A. H. Manganese Compounds. In *Ullmann's Encyclopedia of Industrial Chemistry*; Elvers, B., Ed.; John Wiley and Sons: New York, 2000.
- (52) Gorlin, Y.; Jaramillo, T. F. Investigation of Surface Oxidation Processes on Manganese Oxide Electrocatalysts using Electrochemical Methods and ex situ X-ray Photoelectron Spectroscopy. *J. Electrochem. Soc.* **2012**, *159*, H782–H786.
- (53) McBreen, J. The Electrochemistry of  $\beta$ -MnO<sub>2</sub> and  $\gamma$ -MnO<sub>2</sub> in Alkaline Electrolyte. *Electrochim. Acta* **1975**, 20, 221–225.
- (54) Sheng, W.; Gasteiger, H. A.; Shao-Horn, Y. Hydrogen Oxidation and Evolution Reaction Kinetics on Platinum: Acid vs. Alkaline Electrolytes. *J. Electrochem. Soc.* **2010**, *157*, B1529–B1536.
- (55) Baturina, O. A.; Aubuchon, S. R.; Wynne, K. J. Thermal Stability in Air of Pt/C Catalysts and PEM Fuel Cell Catalyst Layers. *Chem. Mater.* **2006**, *18*, 1498–1504.